Published in final edited form as:
Cancer Res. 2016 January 1; 76(1): 43–49. doi:10.1158/0008-5472.CAN-15-0934.

Non-invasive quantification of 2-hydroxyglutarate in human gliomas with IDH1 and IDH2 mutations

Uzay E Emir[1], **Sarah J Larkin**[2], **Nick de Pennington**[2,3], **Natalie Voets**[1], **Puneet Plaha**[3], **Richard Stacey**[3], **Khalid Al-Qahtani**[4], **James Mccullagh**[4], **Christopher J Schofield**[4], **Stuart Clare**[1], **Peter Jezzard**[1], **Tom Cadoux-Hudson**[3,*], and **Olaf Ansorge**[2,*]

[1]The FMRIB Centre, Nuffield Department of Clinical Neurosciences, University of Oxford, John Radcliffe Hospital, Oxford, OX3 9DU, United Kingdom

[2]Nuffield Department of Clinical Neurosciences, University of Oxford, Oxford, United Kingdom

[3]Department of Neurosurgery, John Radcliffe Hospital, Oxford University Hospitals NHS Trust, Oxford, United Kingdom

[4]Department of Chemistry, University of Oxford, Oxford, OX1 3TA, United Kingdom

Abstract

Mutations in the isocitrate dehydrogenase genes (IDH1/2) occur often in diffuse gliomas where they are associated with abnormal accumulation of the oncometabolite 2-hydroxyglutarate (2-HG). Monitoring 2-HG levels could provide prognostic information in this disease, but detection strategies that are non-invasive and sufficiently quantitative have yet to be developed. In this study, we address this need by presenting a proton magnetic resonance spectroscopy (^{1}H MRS) acquisition scheme that uses an ultra-high magnetic field (≥7T) capable of noninvasively detecting 2-HG with quantitative measurements sufficient to differentiate mutant cytosolic IDH1 and mitochondrial IDH2 in human brain tumors. Untargeted metabolomics analysis of in vivo ^{1}H MRS spectra discriminated between IDH mutant tumors and healthy tissue and separated IDH1 from IDH2 mutations. High-quality spectra enabled the quantification of neurochemical profiles

[*]**Corresponding author:** Uzay Emrah Emir, Oxford Centre for Functional MRI of the Brain (FMRIB), John Radcliffe Hospital, Headington, Oxford OX3 9DU, UK tel +44 (0) 1865 222769 fax +44 (0) 1865 222717 uzay.emir@ndcn.ox.ac.ukhttp://www.fmrib.ox.ac.uk/research/mr-spectroscopy.
[*]**Co-senior authors**

Author contributions

UEE conceived, designed, performed the experiments and wrote the paper. SJL, OA, NDP, NV designed and performed experiments and contributed to writing the paper. PP, RS, KAQ, JM, CJS, SC and PJ reviewed the paper. TCH and OA conceived the study, designed the experiments and wrote the paper.

SJL sarah.larkin@ndcn.ox.ac.uk
NDP nick.depennington@ndcn.ox.ac.uk
NV natalie.voets@ndcn.ox.ac.uk
PP Puneet.Plaha@ouh.nhs.uk
RS Richard.Stacey@ouh.nhs.uk
KAQ khalid.al-qahtani@hertford.ox.ac.uk
JM james.mccullagh@chem.ox.ac.uk
CJS christopher.schofield@chem.ox.ac.uk
SC stuart.clare@ndcn.ox.ac.uk
PJ peter.jezzard@ndcn.ox.ac.uk
TCH Tom.Cadoux-Hudson@ouh.nhs.uk
OA olaf.ansorge@ndcn.ox.ac.uk

Competing Interests A patent application related to the presented work has been filed by UEE.

Europe PMC Funders Author Manuscripts

consisting of at least eight metabolites, including 2-HG, glutamate, lactate, and glutathione in both tumor and healthy tissue voxels. Notably, IDH2 mutation produced more 2-HG than IDH1 mutation, consistent with previous findings in cell culture. By offering enhanced sensitivity and specificity, this scheme can quantitatively detect 2-HG and associated metabolites that may accumulate during tumor progression, with implications to better monitor patient responses to therapy.

Keywords

isocitrate dehydrogenase; MRS; glioma; ultra-high field; 2-HG

Introduction

Mutations in isocitrate dehydrogenase (IDH) 1 and 2 occur in over 80% of low-grade gliomas and secondary glioblastomas(1). Wildtype IDH catalyzes the conversion of isocitrate to α-ketoglutarate (α-KG); IDH1 (cytosolic) and IDH2 (mitochondrial) mutant tumors accumulate 2-hydroxyglutarate (2-HG) as a result of a neomorphic IDH activity, which additionally catalyses reduction of α-KG to give 2-HG (Fig. 1a) (2,3). The role of 2-HG in gliomagenesis is uncertain, but 2-HG is recognised as a tumor-specific biomarker and a potential target for pharmacological intervention (4). It is proposed that different subtypes of IDH mutations might be distinguished on the basis of their characteristic neurochemical profiles.

To date, immunohistochemical (IHC) and molecular pathological analysis of surgically obtained tumor tissue is required to diagnose an IDH mutated glioma. Recently, the detection of 2-HG with high-resolution magic angle spinning ^{1}H-MRS was demonstrated, followed by *in vivo* detection of ^{1}H-MRS at 3T (5,6). However, due to overlapping multiplets from glutamate (Glu), glutamine (Gln), glutathione (GSH) and γ-aminobutyric acid (GABA), reliable measurement of 2-HG at field strengths of 3T and below is difficult and cannot attribute the 2-HG signal to either the activity of IDH1 or IDH2 mutations. At ultra-high magnetic fields (UHF, ≥7T), *in vivo* ^{1}H-MRS detection of metabolites benefits from substantial gains in signal-to-noise ratio (SNR) and spectral resolution, enabling the detection of subtle changes in metabolite levels from small volumes-of-interest (VOIs) and higher specificity than at 3T (7). Thus, *in vivo* ^{1}H-MRS of 2-HG and associated metabolites at UHF offers the possibility to make important contributions not only in the early differential diagnosis of brain tumors, but also more importantly in assisting the study of disease progression and treatment response that cannot be obtained with other methods.

In this study, we show a proton magnetic resonance spectroscopy (^{1}H-MRS) acquisition scheme enabling discernible 2-HG in the spectra of IDH-mutant patients within 20s and quantify metabolic changes associated with the IDH mutation. Due to the increased sensitivity and specificity of this scheme at UHF, we demonstrate elevated 2-HG accumulation in IDH2 R172K (mitochondrial) compared to the IDH1 R132H (cytosolic) mutant tumors in human brains noninvasively.

Europe PMC Funders Author Manuscripts

Materials and Methods

Subject Inclusion

Fourteen glioma patients (8 men, 45±13 years old, mean±SD) and 8 healthy volunteers (6 men, 42±11 years old) participated in the study after giving written informed consent (Table 1). One patient (P005) was excluded due to poor placement of a dielectric pad resulting in high measurement noise and insufficient transmit field. The Oxfordshire B National Research Ethics Committee approved the study.

Immunohistochemistry and DNA Sequencing

Immunohistochemistry and DNA sequencing are detailed in Supplementary Methods.

MR imaging and spectroscopy

Each volunteer participated in a 1 hour MR scan. MR experiments were performed using a 7T whole body MR system (Siemens, Erlangen) with a Nova Medical 32-channel receive array head-coil. VOIs were defined on each participant's anatomical scan (1-mm isotropic resolution MPRAGE sequence: repetition time TR = 2.3 s, inversion time TI = 1.05 s, echo time TE = 2.8 ms, total acquisition time = 3 min). First- and second-order shims were first adjusted by gradient-echo shimming (8). The second step involved only fine adjustment of first order shims using FASTMAP (9). Barium titanate pads were used to increase the extent of the effective transmit field (B_1^+) (10). Spectra were measured with a semi-localization by adiabatic selective refocusing (semi-LASER)(11) pulse sequence (TE = 110 ms, TR = 5-6 s, number of transients NT = 128, spectral bandwidth = 6 kHz, data points = 2048) with VAPOR (variable power and optimized relaxation delays) water suppression and outer volume suppression (OVS). The distance between the voxel edge and each OVS saturation band was set to 8 mm, thus ensuring no signal loss due to OVS bands. For patients, volumes of 8 ml (20×20×20 mm^3) were acquired from the tumor and, where time allowed, contralateral healthy tissue regions. Tumor voxel positioning aimed to exclude very heterogeneous tissue and minimize inclusion of healthy-appearing tissue (except in one previously-operated patient (P002), a 2 ml (20×10×10 mm^3) volume was measured). For healthy volunteers, an 8 ml voxel was placed in regions similar to the patient tumor locations.

Simulations

The model spectra of 2-HG and other metabolites were generated based on previously reported chemical shifts and coupling constants (12,13) using the GAMMA/PyGAMMA simulation library of VESPA (14) for carrying out the density matrix formalism. 2-Hydroxyglutarate (2-HG) contains five C-H protons which are detectable by magnetic resonance spectroscopy (MRS) and which have the following chemical shifts (δ_{Hn}) and scalar coupling constants in H_2O ($J_{Hn\text{-}Cm}$) (13): δ_{H2}=4.022, δ_{H3}=1.825, $\delta_{H3'}$= 1.977, δ_{H4}= 2.221, $\delta_{H4'}$= 2.272, $J_{H2\text{-}H3}$=7.6, $J_{H2\text{-}H3'}$=4.1, $J_{H2\text{-}H4}$=0, $J_{H2\text{-}H4'}$ =0, $J_{H3\text{-}H3'}$=−14.0, $J_{H3\text{-}H4}$=5.3, $J_{H3\text{-}H4'}$=10.4, $J_{H3'\text{-}H4}$=10.6, $J_{H3'\text{-}H4'}$=6.0, $J_{H4\text{-}H4'}$=−15.0. Simulations were performed with the same RF pulses and sequence timings as that on the 7T system in use. The echo time and timing between RF pulses influences the lineshape of 2-HG and therefore

simulations were performed to obtain the best inter-pulse delays for an optimal 2-HG detection at 7T. Thus, 2-HG was simulated for varied inter-pulse delays using 20 equally spaced steps between 8-46 ms, 14-109 ms and 8-103 ms for TE_1, TE_2 and TE_3, respectively.

Spectral Processing

Spectral processing steps are detailed in Supplementary Methods.

Untargeted Metabolomics Analysis

After transforming the pre-processed signals to the frequency domain, the baseline offset was subtracted from the spectrum. The normalization of the spectral data vector to the L2-norm was performed based on the data-points in the region [1.6, 4.2] ppm. Finally, a spectral range restricted to [1.6, 3.1] ppm was used as an input to SpectraClassifier 3.1, an automated MRS- based classifier-development system (15). Feature selection was performed with Correlation-based Feature Subset Forward Selection and the resulting features were used as an input to a Fisher Linear Discriminant Analysis (LDA). The number of spectral features selected using correlation analysis was set to 2 ($<n/3$, where n is the number of cases in the smallest group).

Spectral Quantification

LCModel (16) fitting using a basis set simulated at TE of 110ms was performed over the spectral range from 0.5 to 4.2 ppm for pre-processed signals (Supplementary Figure 1). The metabolite concentrations were estimated with respect to a water reference. Only the transverse (T_2) relaxation effects of the water signal were corrected for tumor and healthy tissue using published water T_2 values for healthy tissue voxels (T_2 = 50ms), and assuming that the T_2 of water in tumor tissue is 2× longer than in healthy tissue (17). The relaxation effects of metabolites and fraction of CSF in the voxel were neglected. CRLBs (estimated error of the metabolite quantification) of LCModel analysis were used to evaluate the sensitivity of metabolite quantification at 7T. Metabolites quantified with CRLB above 30% were classified as not reliably detected. Only metabolites quantified with CRLB ≤ 30% in at least half of the spectra from a tissue were included in the final neurochemical profile. If the correlation between two metabolites was consistently high (correlation coefficient <−0.5), their sum was reported, such as Glc + Tau, NAA + NAAG (tNAA, total NAA), Cr + PCr (tCr, total creatine), GPC + PCho (tCho, total choline).

Results and Discussion

Due to its minimal chemical shift displacement error and insensitivity to transmit field (B_1^+) inhomogeneities at UHF, we investigated the semi-localization by adiabatic selective refocusing sequence (semi-LASER)(11) for *in vivo* 2-HG detection (Fig. 1b). We conducted density matrix simulations to establish the optimal inter-pulse delays of the semi-LASER sequence for 2-HG detection (Fig. 1c). The simulations indicate that the 2-HG multiplets at 2.25 ppm (H4, H4′) lead to a maximum absorptive negative (inverted) multiplet at a total echo time of 100–120 ms (Fig. 1c). A TE of 110 ms was chosen, since simulations showed a near fully absorptive negative 2-HG (Supplementary Figure 2) and lactate (Lac) spectral pattern at 2.25 ppm and 1.35 ppm with timings TE_1= 11 ms, TE_2 = 65 ms and TE_3=34 ms

(total TE=110ms). The accuracy of simulation and specificity of the proposed acquisition scheme was tested on three 'phantoms', which contained 2-HG with glycine (Gly), Lac with acetate (Ace) and 2-HG (4 mM) with Glu (4 mM), Gln (4 mM), NAA (10 mM) and Gly (10 mM). The spectral shape of 2-HG and Lac at TE=110ms obtained from these phantom experiments closely resembled the simulated 2-HG and Lac shape determined by LCModel (16) fitting (Supplementary Figure 3). In comparison to the shortest achievable TE of 36 ms, a TE of 110 ms resulted in 2.9 (simulation) and 1.5 (phantom) fold higher 2-HG signal at 2.25 ppm, respectively (Supplementary Figure 4). In addition, Fig. 1d illustrates phantom spectra of 2-HG, Gln, Glu and NAA obtained with semi-LASER at TE = 36 (TE_1 =11 ms, TE_2 = 15 ms and TE_3 = 10 ms) and TE = 110 ms, together with LCModel fits. The LCModel analysis of a phantom consisting of 2-HG, Gln, Glu, NAA and Gly at TE = 110 ms resulted in CRLBs of 4%, 4%, 9%, 1% and 1%, respectively whereas at TE 36 ms the CLRBs were 5%, 3%, 3%, 1% and 1%, respectively. Quantitative comparison of short and long TEs using the ratio of 2-HG to the sum of Glu+Gln resulted in values of 0.56 and 0.44, respectively, which was similar to the prepared concentration ratio of 0.5. Although spectral overlap with the adjacent resonances of Glu, Gln and 2-HG was more prominent at TE = 36 ms, the CLRB values of 2-HG at 36 ms was similar that of at 110 ms. This was due to the H4 proton of 2-HG at 4.01 ppm, which was hard to detect under *in vivo* conditions due to overlapping peaks of myo-inositol (*myo*-Ins) at 4.05 ppm, Lac at 4.09 ppm and tCr 3.91 ppm. In order to determine the effect of the H4 proton of 2-HG on the CRLBs, an additional LCModel analysis between 3.9 and 0.5 ppm resulted in an increased CRLB of 2-HG at TE =36 ms (CRLB, 8%) compared to that of TE = 110 ms (CRLB, 4%) (Supplementary Figure 5).

Ten of 14 patients studied with *in vivo* MRS were shown to have mutations of IDH in tumor tissue subsequently obtained at surgery (Fig. 2a and Table 1). Tissue samples underwent IHC analysis for the common IDH1 R132H mutation. Cases that were IDH1 R132H immunonegative were subjected to DNA sequencing. Three immunonegative cases (P006, P012 and P014) harboured a less common IDH2 R172K mutation detectable in the sequencing electropherogram.

Figure 2b shows representative spectra from three different patients (P006, P010 and P011) obtained from contralateral healthy tissue and tumor voxels at 7T. In all cases, the residual water signal was smaller than the major metabolite peaks tCho and tNAA for tumor and healthy tissue voxels, respectively). In addition, the double localization accomplished by semi-LASER and OVS eliminated signals from outside the VOI, such as lipid signals from the subcutaneous tissue, resulting in artefact-free spectra with a flat baseline in the spectral range [1.6, 4.2] ppm for all subjects (Fig. 2c).

Given the phantom and *in vivo* measurements, we then characterized the spectral pattern changes induced by the IDH mutations, particularly any visually discernible 2-HG signal. Thus, untargeted metabolomics analysis was performed for the spectral range restricted to [1.6, 3.1] ppm. The untargeted feature extraction of *in vivo* spectra from healthy and tumor voxels resulted in a spectral pattern deviation at 2.25 ppm, where the 2-HG peak is located (Fig. 2c). The feature identified was used for LDA to separate data into IDH mutant or healthy subjects. The LDA classifier projection space plot identified distinct clustering

patterns, not only distinguishing 7T MRS spectra between IDH mutant tumors and healthy tissue but, furthermore, separating IDH1 R132H from IDH2 R172K mutations (Fig. 2d).

In order to characterize this difference in more detail, we quantified 2-HG and related metabolite concentrations using LCModel (16), which uses an *a priori* established basis set for a selected group of metabolites (Supplementary Figure 1). The high spectral quality enabled the quantification of a neurochemical profile consisting of 8 metabolites in both tumor and healthy tissue voxels (Fig. 3b). A 2-HG signal was *only* detected in patients exhibiting IDH1 R132H and IDH2 R172K mutations. We demonstrated that mitochondrial IDH2 R172K mutations lead to higher levels of 2-HG than cytosolic IDH1 R132H mutations (9.06 ± 0.87 and 2.53 ± 0.75 μmol/g, respectively) (Fig. 3c), in agreement with a previous cell culture findings (2). In addition, high Lac, *myo*-Ins, tCho and Glc+Tau concentrations were observed in tumor voxels, whereas Glu and tNAA were decreased (Fig. 3b). 2-HG concentrations were also evaluated relative to the tCr and tCho, MRS markers for cellular bioenergetics and proliferation (18), respectively (Fig. 3d). The 2-HG ratios (2-HG:tCr and 2-HG:tCho) appeared to be higher in IDH2 R172K compared to the IDH1 132H due to increased 2-HG levels in IDH2 172K. However, for one IDH2 R172K patient, the increase in 2-HG:tCr resulted not only from increased 2-HG but also decreased tCr.

Analysis of CRLBs as a function of the number of signal averages clearly showed that the estimated quantification error per number of transients was always less than for previously published data at 3T (Fig. 3d). Importantly, due to the improved SNR and sensitivity at 7T, the proposed method enabled us to quantify 2-HG in the tumor VOI with a mean CRLB of 16±8.4% following only 4 transient averages (~20 s experimental duration).

We acknowledge that our study is limited by a small sample size, particularly concerning the IDH2 mutations. However, distinction between canonical IDH1 and IDH2 mutation appeared robust even when correcting for tCr and tCho values, and the low frequency of IDH2 mutations in our single-centre study was expected as only 3% of diffuse gliomas of WHO grade II or III carry IDH2 mutations (19). A multi-centre study is required for robust comparisons between canonical and non-canonical IDH1 mutations and IDH2 mutations. One potential limitation of the methodology of this study is the semi-quantification of metabolite levels by using an internal reference method within the same voxel since the effects of tumor heterogeneity, regional differences in absolute and relative metabolite concentrations of water, and metabolite relaxation times are not practical to assess in patient studies. In particular, differences in water and metabolite T_2s with tumor type and grade have the potential to complicate quantification of metabolite concentrations (20). Finally, the use of a single TE of 110 ms, at which overlapping peaks of Glu and Gln are decreased relative to 2-HG at 2.25 ppm, could lead to the underestimation of Glu and Gln concentrations.

A number of studies have demonstrated *in vivo* detection of 2-HG in IDH-mutant tumors at 3T (5,6), commonly used in the clinical setting. However, the assignment of 2-HG resonances at 3T is an important technical challenge not only because of the complex spin-coupling features of overlapping resonances but also due to the lack of SNR and spectral resolution. As we demonstrate, the increased sensitivity and spectral resolution at 7T

substantially improves the precision of *in vivo* detection of 2-HG and other metabolite changes. Finally, non-invasive discrimination between IDH1 and IDH2 mutations with the acquisition scheme should be extended to larger sample sizes to explore new diagnostic and therapeutic approaches and associated metabolite biomarkers.

Supplementary Material

Refer to Web version on PubMed Central for supplementary material.

Acknowledgements

The research was funded by the National Institute for Health Research (NIHR) Oxford Biomedical Research Centre based at Oxford University Hospitals NHS Trust and the University of Oxford (SJL, OA). The views expressed are those of the author(s) and not necessarily those of the NHS, the NIHR or the Department of Health. We acknowledge the Oxford Brain Bank, supported by the Medical Research Council (MRC), Brains for Dementia Research (BDR), the Wellcome Trust (UEE), the Dunhill Medical Trust (PJ) and the NIHR Oxford Biomedical Research Centre.

References

1. Parsons DW, Jones S, Zhang X, Lin JC, Leary RJ, Angenendt P, et al. An integrated genomic analysis of human glioblastoma multiforme. Science. 2008; 321:1807–12. [PubMed: 18772396]
2. Ward PS, Lu C, Cross JR, Abdel-Wahab O, Levine RL, Schwartz GK, et al. The potential for isocitrate dehydrogenase mutations to produce 2-hydroxyglutarate depends on allele specificity and subcellular compartmentalization. J Biol Chem. 2013; 288:3804–15. [PubMed: 23264629]
3. Dang L, White DW, Gross S, Bennett BD, Bittinger MA, Driggers EM, et al. Cancer-associated IDH1 mutations produce 2-hydroxyglutarate. Nature. 2009; 462:739–44. [PubMed: 19935646]
4. Yen KE, Bittinger MA, Su SM, Fantin VR. Cancer-associated IDH mutations: biomarker and therapeutic opportunities. Oncogene. 2010; 29:6409–17. [PubMed: 20972461]
5. Choi C, Ganji SK, DeBerardinis RJ, Hatanpaa KJ, Rakheja D, Kovacs Z, et al. 2-hydroxyglutarate detection by magnetic resonance spectroscopy in IDH-mutated patients with gliomas. Nat Med. 2012; 18:624–9. [PubMed: 22281806]
6. Andronesi OC, Kim GS, Gerstner E, Batchelor T, Tzika AA, Fantin VR, et al. Detection of 2-hydroxyglutarate in IDH-mutated glioma patients by in vivo spectral-editing and 2D correlation magnetic resonance spectroscopy. Sci Transl Med. 2012; 4:116ra4.
7. Mekle R, Mlynarik V, Gambarota G, Hergt M, Krueger G, Gruetter R. MR spectroscopy of the human brain with enhanced signal intensity at ultrashort echo times on a clinical platform at 3T and 7T. Magn Reson Med. 2009; 61:1279–85. [PubMed: 19319893]
8. Shah, S.; Kellman, P.; Greiser, A.; Weale, P.; Zuehlsdorff, S.; Jerecic, R. Rapid Fieldmap Estimation for Cardiac Shimming. Proceedings 17th Scientific Meeting, International Society for Magnetic Resonance in Medicine; Honolulu. 2009; p. 565
9. Gruetter R, Tkac I. Field mapping without reference scan using asymmetric echo-planar techniques. Magn Reson Med. 2000; 43:319–23. [PubMed: 10680699]
10. Teeuwisse WM, Brink WM, Haines KN, Webb AG. Simulations of high permittivity materials for 7 T neuroimaging and evaluation of a new barium titanate-based dielectric. Magn Reson Med. 2012; 67:912–8. [PubMed: 22287360]
11. van de Bank BL, Emir UE, Boer VO, van Asten JJ, Maas MC, Wijnen JP, et al. Multi-center reproducibility of neurochemical profiles in the human brain at 7 T. NMR Biomed. 2015; 28:306–16. [PubMed: 25581510]
12. Govindaraju V, Young K, Maudsley AA. Proton NMR chemical shifts and coupling constants for brain metabolites. NMR Biomed. 2000; 13:129–53. [PubMed: 10861994]
13. Bal D, Gryff-Keller A. 1H and 13C NMR study of 2-hydroxyglutaric acid and its lactone. Magnetic Resonance in Chemistry. 2002; 40:533–36.

14. Soher, BJ.; Semanchuk, P.; Todd, D.; Steinberg, J.; Young, K. Vespa: Integrated applications for RF pulse design, spectral simulation and MRS data analysis. Proceedings 19th Scientific Meeting, International Society for Magnetic Resonance in Medicine; Quebec, Canada. 2011; p. 1410

15. Ortega-Martorell S, Olier I, Julia-Sape M, Arus C. SpectraClassifier 1.0: a user friendly, automated MRS-based classifier-development system. BMC Bioinformatics. 2010; 11:106. [PubMed: 20181285]

16. Provencher SW. Automatic quantitation of localized in vivo 1H spectra with LCModel. NMR Biomed. 2001; 14:260–4. [PubMed: 11410943]

17. Isobe T, Matsumura A, Anno I, Yoshizawa T, Nagatomo Y, Itai Y, et al. Quantification of cerebral metabolites in glioma patients with proton MR spectroscopy using T2 relaxation time correction. Magn Reson Imaging. 2002; 20:343–9. [PubMed: 12165353]

18. Oz G, Alger JR, Barker PB, Bartha R, Bizzi A, Boesch C, et al. Clinical proton MR spectroscopy in central nervous system disorders. Radiology. 2014; 270:658–79. [PubMed: 24568703]

19. Hartmann C, Meyer J, Balss J, Capper D, Mueller W, Christians A, et al. Type and frequency of IDH1 and IDH2 mutations are related to astrocytic and oligodendroglial differentiation and age: a study of 1,010 diffuse gliomas. Acta Neuropathol. 2009; 118:469–74. [PubMed: 19554337]

20. Li Y, Srinivasan R, Ratiney H, Lu Y, Chang SM, Nelson SJ. Comparison of T(1) and T(2) metabolite relaxation times in glioma and normal brain at 3T. J Magn Reson Imaging. 2008; 28:342–50. [PubMed: 18666155]

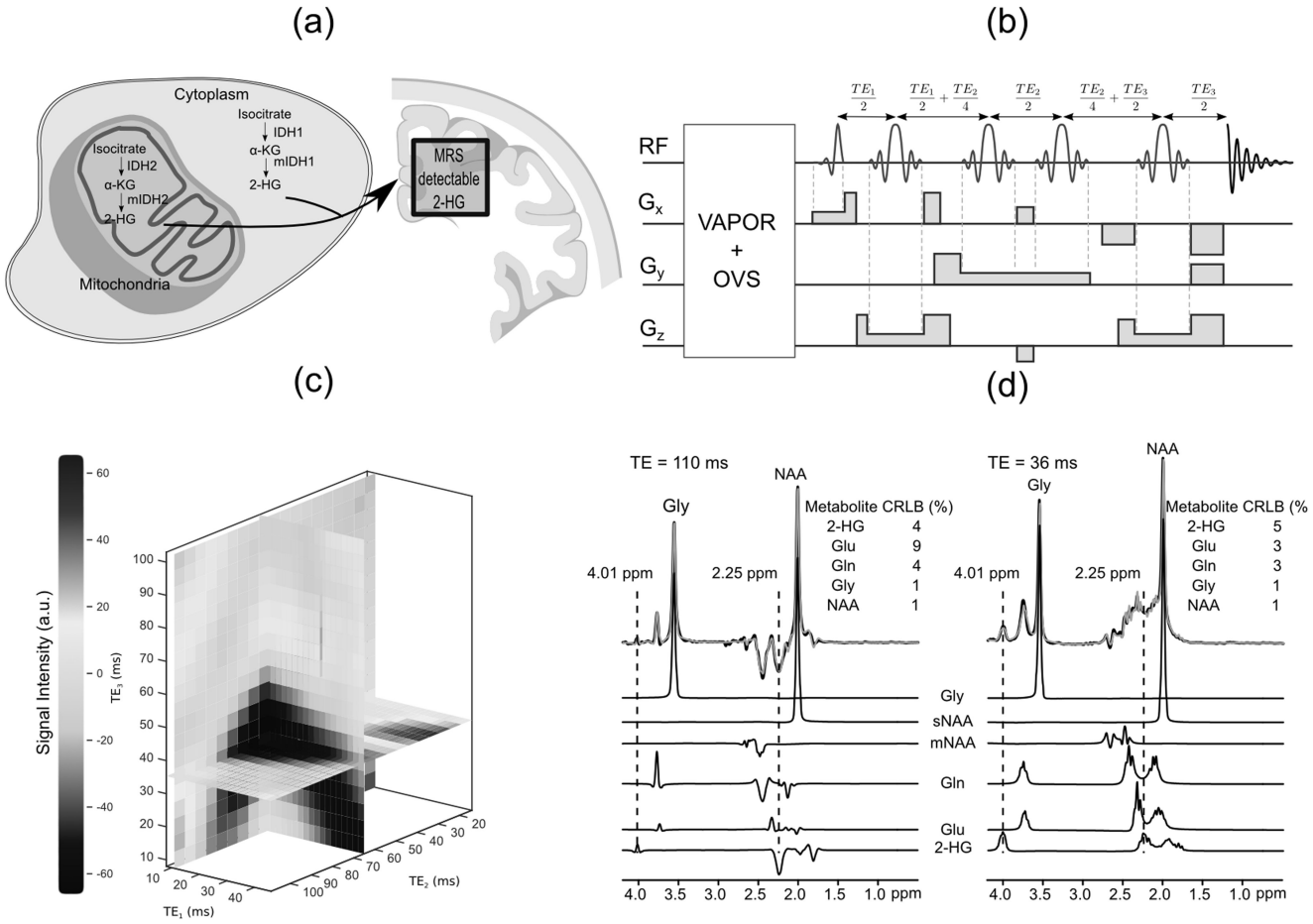

Figure 1. General layout of 2-hydroxyglutarate (2-HG) accumulations and its detection by semi-LASER ^{1}H MRS at 7T

(a) Tumors with *IDH1/2* mutations (mIDH1/2) produce 2-HG in mitochondria and the cytosol and (b) a diagram of the '*in vivo*' ^{1}H-MRS pulse sequence using adiabatic slice selective refocusing pulses (semi-LASER(11)) optimized for 2-HG signal detection. The semi-LASER sequence consists of a 90° excitation pulse (6ms) followed by two couples of adiabatic refocusing pulses (each 6ms). G_x, G_y, and G_z are gradients in read, phase encoding, and slice selection directions, respectively. B_1 indicates RF pulses. (c) By using GAMMA/PyGAMMA simulation library of VESPA(14) to carry out the density matrix formalism, time delays between the RF pulses are tuned to optimum 2-HG detection. At the echo time (TE)= 110 ms (TE_1 =11 ms, TE_2 = 65 ms and TE_3 = 34 ms), the one of the multiplets of 2-HG at ~2.25 (H4, H4′) was fully absorptive with a negative spectral pattern. (d) Phantom spectra of 2-HG, Gln, Glu, NAA and Gly obtained with semi-LASER at TE = 36 (TE_1 =11 ms, TE_2 = 15 ms and TE_3 = 10 ms) and 110 ms, together with LCModel(16) fitting and corresponding Cramér-Rao lower bounds (CRLBs). (TR = 5000 ms; number of transients, 128; volume of interest, 8 ml). Phantom spectra were line broadened to match line widths encountered in vivo.

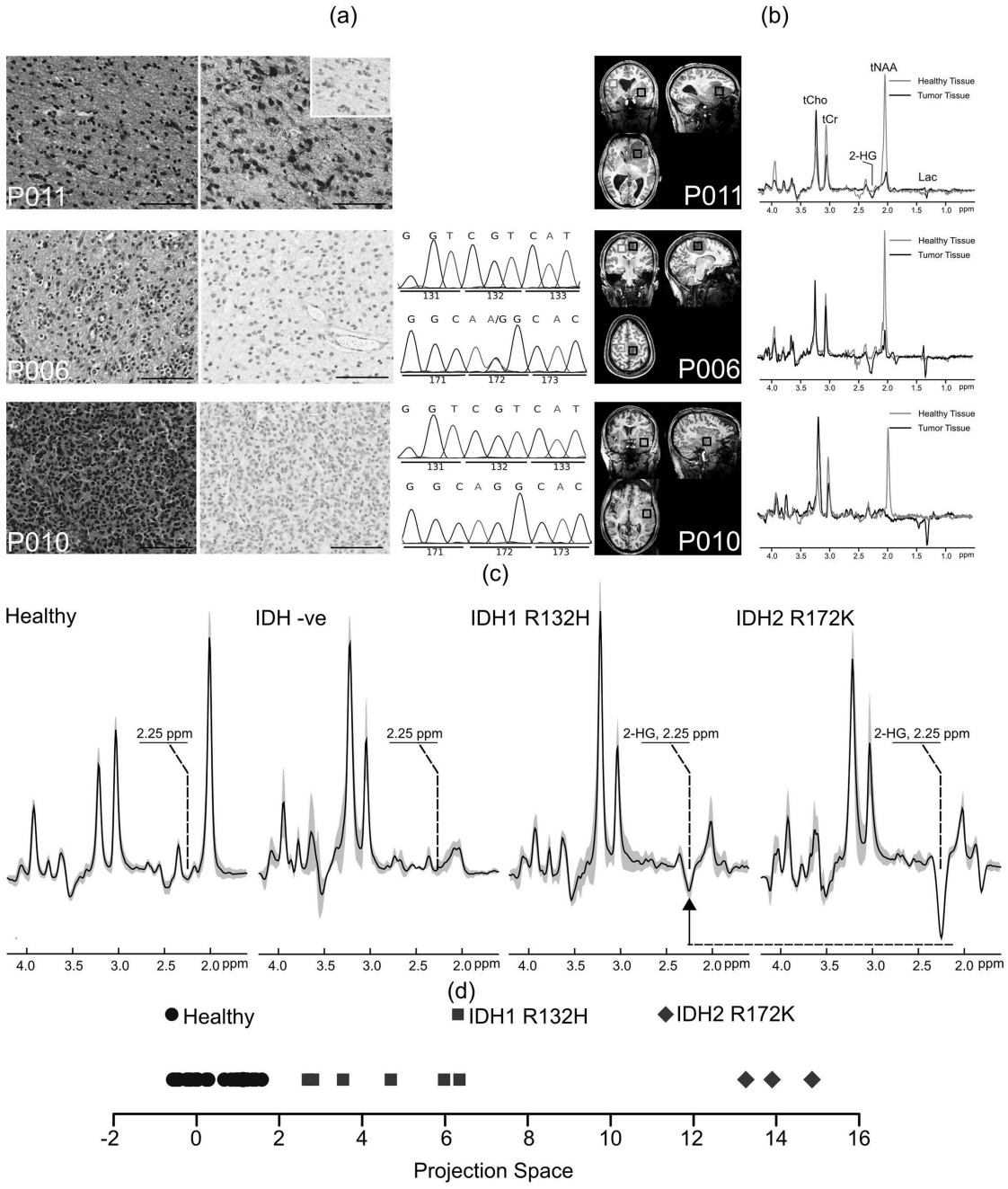

Figure 2. Histology and *in vivo* ^{1}H-MRS at 7T

(a) Haematoxylin and eosin (H&E) stained (left) and Immunohistochemistry with anti-IDH1 R132H antibody (middle (inset, P53)). PCR and direct sequencing of codon 132 of IDH1 (upper trace) and R172 of IDH2 (lower trace) was performed for immunonegative cases (right). All scale bars 100μm. (b) Representative of contralateral healthy and of tumor tissue voxel placement and respective *in vivo* ^{1}H-MRS spectra for immunopositive (top), immunonegative with rare mutation (middle) and a wild type tumor patient (bottom). (c) Mean (solid line) and ±standard deviation (shade) of L2-normalized 1H-MRS spectra from

all subjects. Vertical dashed line indicates the identified spectral feature (2.25 ppm) by untargeted metabolomics analysis. (d) Linear Discriminant Analysis (LDA) latent space for the discrimination of the spectra from tumor tissue voxel of IDH mutant glioma patients and healthy tissue voxel.

Europe PMC Funders Author Manuscripts

Europe PMC Funders Author Manuscripts

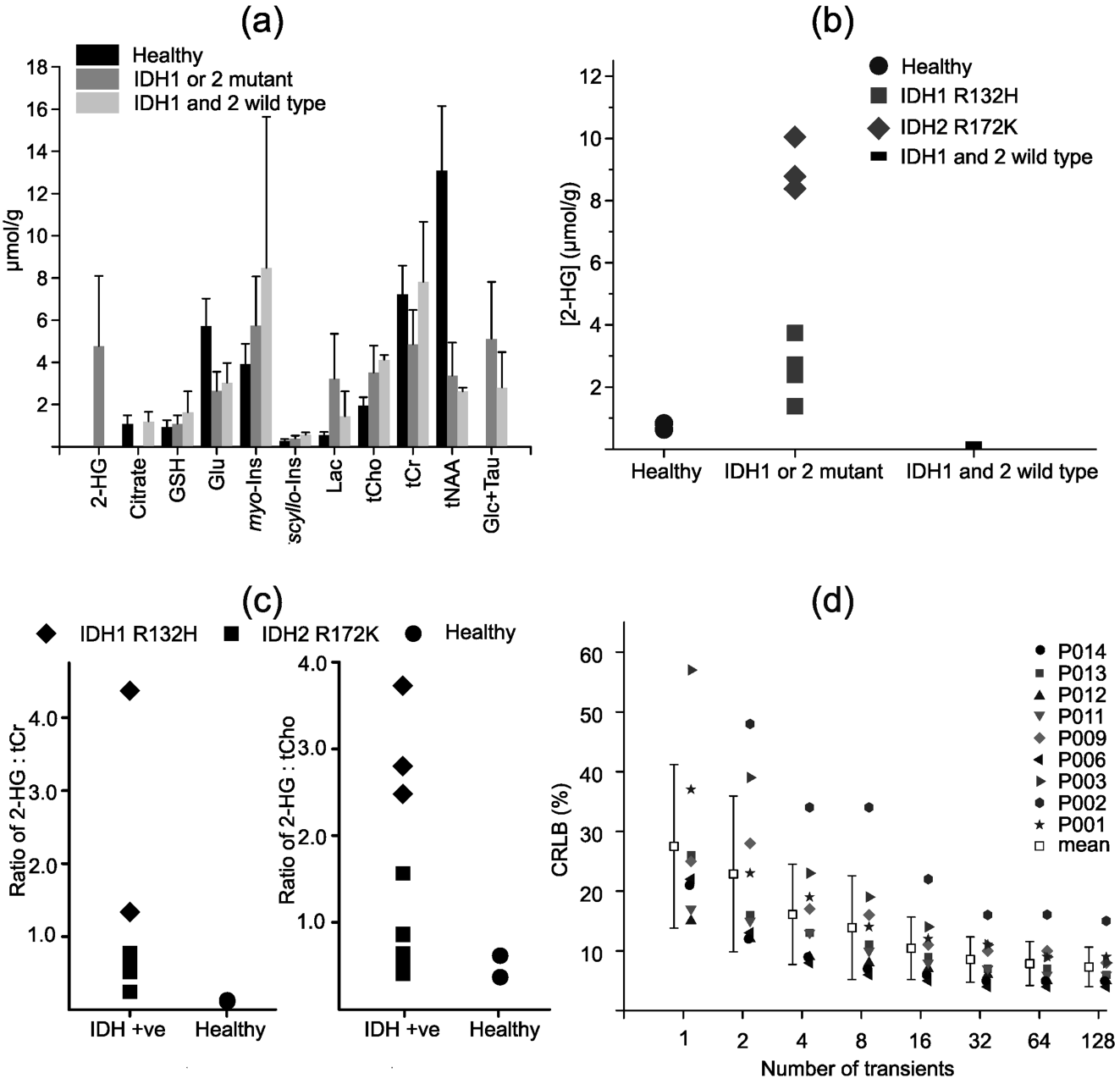

Figure 3. LCModel analysis

(a)Neurochemical profiles determined by LCModel fitting. Only metabolites quantified with Cramér-Rao lower bounds (CRLB) ≤30% in at least half of the spectra from a brain region were included in the profiles. (b) 2-HG concentrations in µmol/g. Only healthy tissue voxels of two patients resulted in 2-HG detection with CLRBs of 25 and 26%, respectively. (c) 2-HG concentrations relative to the tCr and tCho (d) Cramér-Rao lower bounds (CRLBs) of 2-HG detection by LCModel fitting together with means (boxes) and standard deviations (error bars) as a function of the number of transients. Error-bars: inter-subject standard deviation. Glu, glutamate; GSH, glutathione; myo-Ins, myo-inositol; scyllo-Ins, scyllo-

inositol; tNAA, total N-acetylaspartate; tCho, total choline; tCr, total creatine; Glc, glucose; Tau, taurine; Lac, lactate.

Europe PMC Funders Author Manuscripts

Table 1

Demographic and clinical characteristics of patients and healthy volunteer participants who were scanned by *in vivo* ^{1}H-MRS at 7T.In cases where the immunohistochemistry (IHC)did not detect IDH1 R132H mutations, regions containing IDH1 codon 132 and IDH2 codon 172 were PCR amplified and subsequently sequenced to establish whether a mutation was present at either locus. The number of volumes of interest (VOIs) for tumor and healthy tissue islisted for each participant. +ve, immunopositive; −ve, immunonegative; W/T, wild type; WHO, world health organization; NA, not applicable.

SubjetID	Age/gender	Diagnosis	IHC	DNA sequencing	Number of healthy tissue VOIs	Number of tumor tissue VOIs
P001	31/M	Anaplastic astrocytoma (WHO grade 3)	+ve	NA	1	1
P002	36/F	Anaplastic oligoastrocytoma (WHO grade 3)	+ve	NA	1	1
P003	34/M	Anaplastic astrocytoma (WHO grade 3)	+ve	NA	1	1
P004	68/M	Astrocytoma (WHO grade 2)	−ve	W/T	1	1
P005	47/M	Anaplastic astrocytoma (WHO grade 3)	+ve	IDH1(R132H)	1	1
P006	27/F	Oligodendroglioma (WHO grade 2)	−ve	IDH2(R172K)	1	1
P007	52/M	Glioblastoma (WHO grade 4)	−ve	W/T	-	1
P008	54/M	Glioblastoma (WHO grade 4)	−ve	W/T	-	1
P009	51/M	Anaplastic astrocytoma (WHO grade 3)	+ve	NA	1	1
P010	60/F	Glioblastoma (WHO grade 4)	−ve	W/T	1	1
P011	53/F	Astrocytoma (WHO grade 2)	+ve	N/A	1	1
P012	29/F	Oligodendroglioma (WHO grade 2)	−ve	IDH2(R172K)	1	1
P013	45/M	Astrocytoma (WHO grade 2)	+ve	NA	1	1
P014	33/F	Oligodendroglioma (WHO grade 2)	−ve	IDH2(R172K)	1	1
C001	47/M	Healthy volunteer	NA	NA	1	NA
C002	38/F	Healthy volunteer	NA	NA	2	NA
C003	54/F	Healthy volunteer	NA	NA	1	NA
C004	51/M	Healthy volunteer	NA	NA	2	NA
C005	24/M	Healthy volunteer	NA	NA	2	NA
C006	37/M	Healthy volunteer	NA	NA	2	NA
C007	55/M	Healthy volunteer	NA	NA	2	NA
C008	37/M	Healthy volunteer	NA	NA	1	NA